Removing shear artifacts in acoustic anisotropic wave propagation

Huy Le, Stewart A. Levin, Robert G. Clapp, and Biondo Biondi

ABSTRACT

We present a method for removing the shear-wave artifacts that occur in anisotropic modeling under the acoustic approximation. Our method is based on an eigenvalue decomposition of the differential operator in the wavenumber domain. Application in a homogeneous orthorhombic medium shows that the shear wave artifacts are removed completely. Accuracy of the resulting operator is also investigated in different media. We find that as the degree of anisotropy reduces, a more compact operator can be used to achieve an acceptable level of accuracy. We apply the proposed method to a heterogeneous model by using the Lloyd algorithm to select a number of references and computing a table of operators.

INTRODUCTION

Orthorhombic symmetry is a more general type of symmetry than transverse isotropy (TI). This type of symmetry can be found, for example, in fractured media where a set of vertical fractures is embedded in a vertically TI medium (Tsvankin, 2012). Generally, one of the challenges of anisotropic imaging and inversion is the increased number of parameters that characterize the media. In particular, in orthorhombic media there are nine independent elastic parameters that enter into a linear relationship between stresses and strains (Tsvankin, 2012). As a result, the system of wave equations in orthorhombic media couple (quasi) P-wave and S-waves. The acoustic approximation, under which the shear velocities along the coordinate axes are set to zero, reduces the number of medium parameters to six (Alkhalifah, 2003). However, this does not mean that the shear-wave velocity is zero everywhere (Grechka et al., 2004). Consequently, the acoustic approximation introduces artifacts that contaminate P-wave data.

A number of methods have been proposed to remove the shear-wave artifacts. The first method is to put the seismic source in an isotropic medium, for example water (Alkhalifah, 2003). This method, however, limits subsequent imaging applications to marine environments or where the source's surrounding area is known to be isotropic. Another method is to use a finite shear-wave velocity (Fletcher et al., 2009). This method uses a choice of shear velocity that makes the reflection coefficient of shear wave zero everywhere. A satisfactory value of shear velocity can be derived in TI

media but might not be simple in orthorhombic media where shear-wave signatures can only be expressed analytically in symmetry planes (Tsvankin, 2012). The third method to reduce shear-wave artifacts is to solve the Christoffel equation to obtain a dispersion relation corresponding to P-waves, which then can be used to propagate a P-wavefield in the Fourier domain (Zhang et al., 2009) or converted to a system of differential equations and solved numerically (Liu et al. (2009); Zhou et al. (2006)).

The method we propose is also based on solving the Christoffel equation. However, unlike the TI case in which P- and SV-waves decouple from SH-wave and the Christoffel equation can be solved analytically, in orthorhombic media, the solution is computed numerically through an eigenvalue decomposition of the differential operator in the wavenumber domain.

THEORY

Under the acoustic approximation, the system of wave equations in orthorhombic media is:

$$\frac{\partial^2 \boldsymbol{\sigma}}{\partial t^2} = M\mathbf{D}\boldsymbol{\sigma}, \tag{1}$$

where $\boldsymbol{\sigma}$ is a vector of three normal stresses, M is the density-normalized stiffness matrix and is related to Thomsen anisotropy parameters (vertical P-velocity v_{pz}, ϵ, and δ) by:

$$\begin{aligned}
m_{11} &= v_{pz}^2(1+2\epsilon_2),\\
m_{12} &= m_{21} = v_{pz}^2(1+2\epsilon_2)\sqrt{1+2\delta_3},\\
m_{13} &= m_{31} = v_{pz}^2\sqrt{1+2\delta_2},\\
m_{22} &= v_{pz}^2(1+2\epsilon_1),\\
m_{23} &= m_{32} = v_{pz}^2\sqrt{1+2\delta_1},\\
m_{33} &= v_{pz}^2,
\end{aligned} \tag{2}$$

and

$$\mathbf{D} = \begin{bmatrix} \frac{\partial^2}{\partial x^2} & & \\ & \frac{\partial^2}{\partial y^2} & \\ & & \frac{\partial^2}{\partial z^2} \end{bmatrix}. \tag{3}$$

See, for example, Fowler and King (2011) or Zhang and Zhang (2011) for derivations.

After a spatial Fourier transform, the system of equations 1 becomes:

$$\frac{\partial^2 \tilde{\boldsymbol{\sigma}}}{\partial t^2} = M\tilde{\mathbf{D}}\tilde{\boldsymbol{\sigma}}, \tag{4}$$

where now

$$\tilde{\mathbf{D}} = \begin{bmatrix} -k_x^2 & & \\ & -k_y^2 & \\ & & -k_z^2 \end{bmatrix}. \tag{5}$$

In the wavenumber domain, the operator $M\tilde{\mathbf{D}}$ can be decomposed as:

$$M\tilde{\mathbf{D}} = \mathbf{Q}\mathbf{\Lambda}\mathbf{Q}^{-1}, \tag{6}$$

where $\mathbf{\Lambda} = diag\left[\tilde{\boldsymbol{\lambda}}_i(k_x, k_y, k_z)\right]$ is a diagonal matrix of eigenvalues and $\mathbf{Q}$ is a matrix whose columns are the eigenvectors. The eigenvalue decomposition is computed for every (k_x, k_y, k_z), resulting in the eigenvalues and components of the eigenvectors being operators in wavenumber domain.

Define $\tilde{\boldsymbol{\sigma}}^P = \mathbf{Q}^{-1}\tilde{\boldsymbol{\sigma}}$, which is the projection of the stress fields, $\tilde{\boldsymbol{\sigma}}$, onto the row vectors of $\mathbf{Q}^{-1}$. With this change of basis, the system of equations 4 is decoupled into three independent equations:

$$\frac{\partial^2 \tilde{\boldsymbol{\sigma}}^P}{\partial t^2} = \tilde{\boldsymbol{\lambda}}_i(k_x, k_y, k_z)\tilde{\boldsymbol{\sigma}}^P, \tag{7}$$

with $i = 1, 2, 3$. These three equations correspond to one P-wave and two shear wave artifacts. This decoupling enables separation of the desired P-wave from the unwanted shear artifacts.

The above method is based on the one used in full elastic wave-mode separation (Dellinger and Etgen (1990); Yan and Sava (2009)). However, instead of propagating the 3-component vector fields of stresses, $\boldsymbol{\sigma}$, and projecting onto the row vectors of $\mathbf{Q}^{-1}$, we compute the eigenvalue that corresponds to the P-wave and use it to propagate only one scalar wavefield in the wavenumber domain (equations 7). In a degenerate case of equations 4, that of isotropic symmetry, the eigenvalue that corresponds to the P-wave is the Laplacian and the corresponding projection is the pressure wavefield (see Appendix), as one would expect.

Equations 7 can also be solved in the spatial domain as:

$$\frac{\partial^2 \boldsymbol{\sigma}^P}{\partial t^2} = \boldsymbol{\lambda}_i(x, y, z) * \boldsymbol{\sigma}^P, \tag{8}$$

where $\boldsymbol{\lambda}_i(x, y, z)$ are spatial operators and the asterisk denotes convolution. In order to obtain compact $\boldsymbol{\lambda}_i(x, y, z)$, the exact differential operator, $\tilde{\mathbf{D}}$ is approximated by finite differences (FD):

$$\tilde{\mathbf{D}} \approx \tilde{\mathbf{D}}_{FD} = \begin{bmatrix} A_x & & \\ & A_y & \\ & & A_z \end{bmatrix} \tag{9}$$

where:

$$A_i = \sum_{j=1}^{\frac{N}{2}} \frac{2}{d_i^2} c_j \left(cos(jk_i d_i) - 1\right), \tag{10}$$

are wavenumber-domain approximations to the second derivative of an N^{th}-order finite difference with coefficients c_j, and d_i are the discretization sizes. The resulting

spatial operators can then be optionally tapered and truncated to an affordable size for three-dimensional convolution.

Using the eigenvalue decomposition to separate P-wave from shear artifacts consists of the following steps:

1. For all discrete (k_x, k_y, k_z), solve the eigenvalue problem in equation 6 using: the exact differential operator (equation 5) if propagation is carried out in wavenumber-domain; or using the FD approximate differential operator (equation 9) if propagation is carried out in spatial domain.

2. Choose the eigenvalue that corresponds to the P-wavefield, $\tilde{\boldsymbol{\lambda}}_i(k_x, k_y, k_z)$, to obtain an operator in wavenumber domain.

3a. Fourier transform the wavefield into wavenumber domain, apply the above operator, inverse Fourier transform the result back into space, and march in time using equations 7.

3b. Or: Inverse Fourier transform the operator $\tilde{\boldsymbol{\lambda}}_i(k_x, k_y, k_z)$ into space, optionally taper and truncate the resulting operator, and solve equations 8 in spatial domain.

EXAMPLES IN A HOMOGENEOUS MEDIUM

We apply the method to a homogeneous orthohombic media with $v_{pz} = 2000$ m/s, $\epsilon_1 = 0.2$, $\epsilon_2 = 0.15$, $\delta_1 = 0.07$, $\delta_2 = 0.04$, $\delta_3 = 0.02$. Figure 1 shows a snapshot of the unseparated wavefield modeled by solving equations 1 with 8th-order spatial and second-order temporal finite differences. The unseparated wavefield is contaminated with shear artifacts. Figures 2(a) and 2(b) respectively show the separated P-wavefield and the shear artifacts obtained by solving equations 7 in the wavenumber domain. The choice of eigenvalues in equation 6 determines the output wavefield. We observe that all the eigenvalues are non-positive and the P-wave corresponds to the most negative eigenvalue. These figures show that the eigenvalue decomposition (equation 6) provides a virtually complete separation of the P-wavefield from the shear artifacts.

Removal of shear artifacts can also be carried out in the spatial domain using an approximate differential operator (equation 9). Figure 3 shows the accuracy of different orders of approximation. Lower orders would result in a more compact but less accurate operator than higher orders. In this example, we use a 10^{th}-order FD, i.e. $N = 10$. Figure 4 compares the spatial operators that correpond to the P-wave calculated using the exact (equation 5) and approximate (equation 9) derivatives. The operator obtained from approximate derivatives is more compact than the one obtained from exact derivatives. This compact operator is then limited to a size of 21 and used to solve equations 8 in spatial domain. Figure 5 show the solutions to equations 8, in which the shear artifacts are completely removed from the P-wavefield.

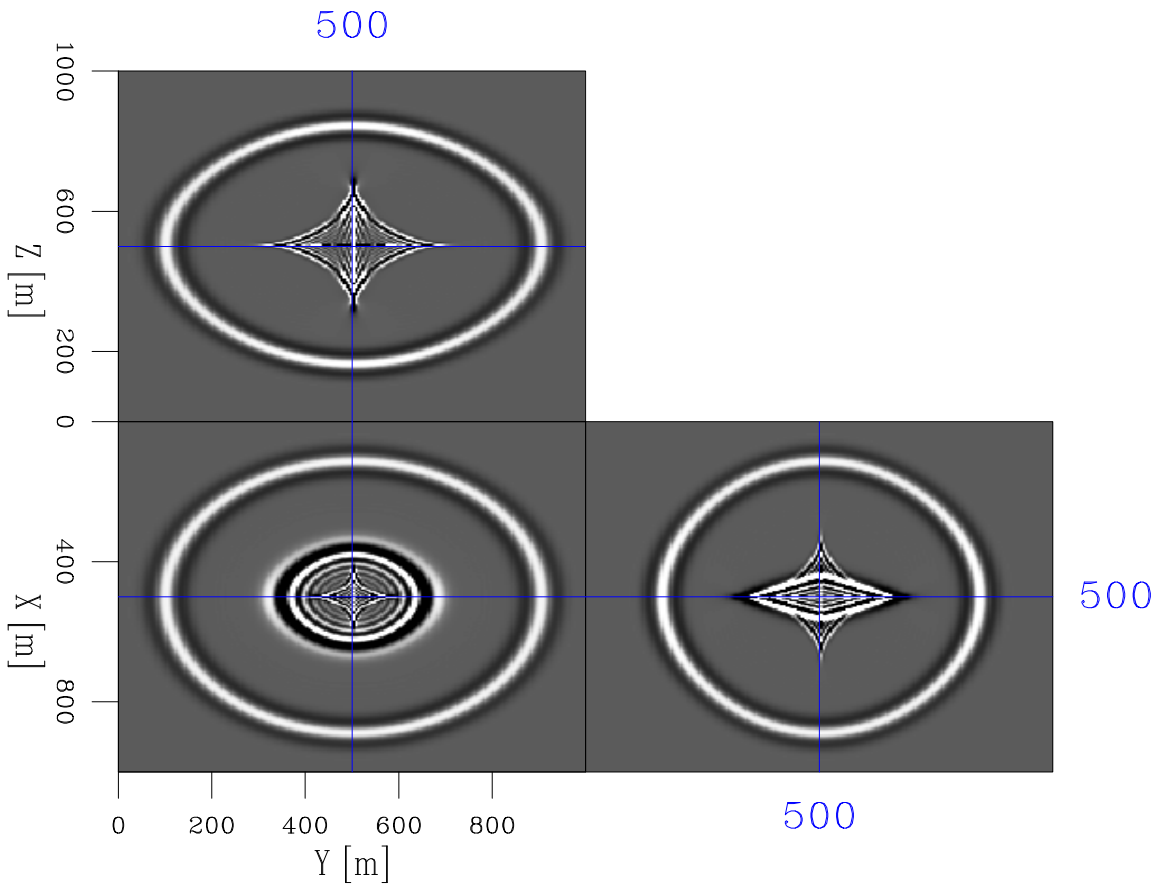

Figure 1: Full unseparated wavefield modeled with equations 1 using 8^{th} order finite difference in space and second order in time. The outer ring is the P-wave while the shear artifacts are in the interior. [**CR**]

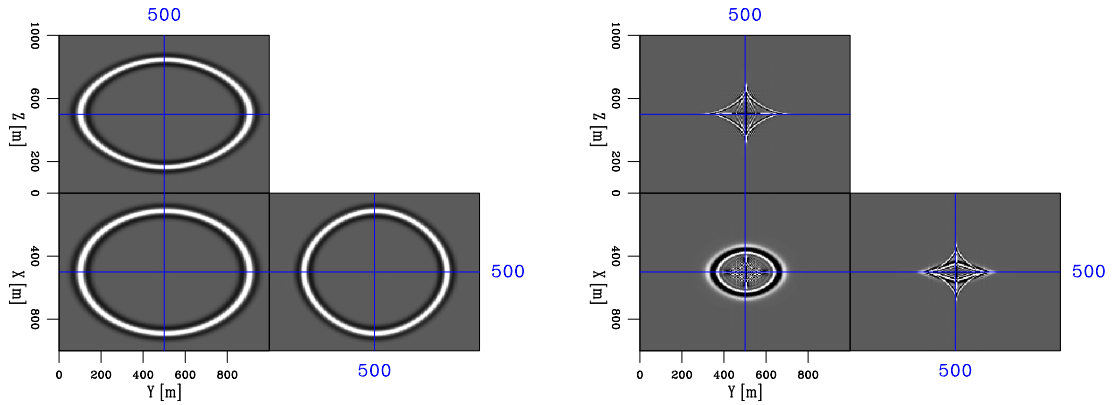

Figure 2: Separated wavefields: (a) P-wavefield and (b) shear artifact modeled by wavenumber-domain propagation (equations 7). [**CR**]

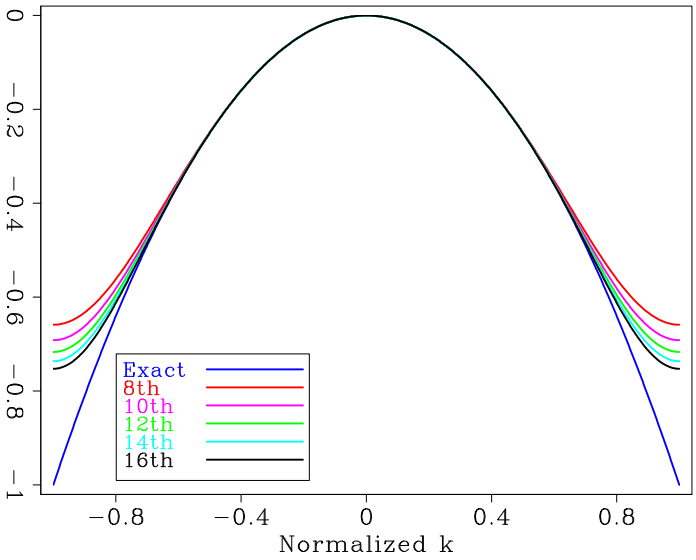

Figure 3: Wavenumber-domain representations of FD approximations to the second derivative of different orders, N. [**ER**]

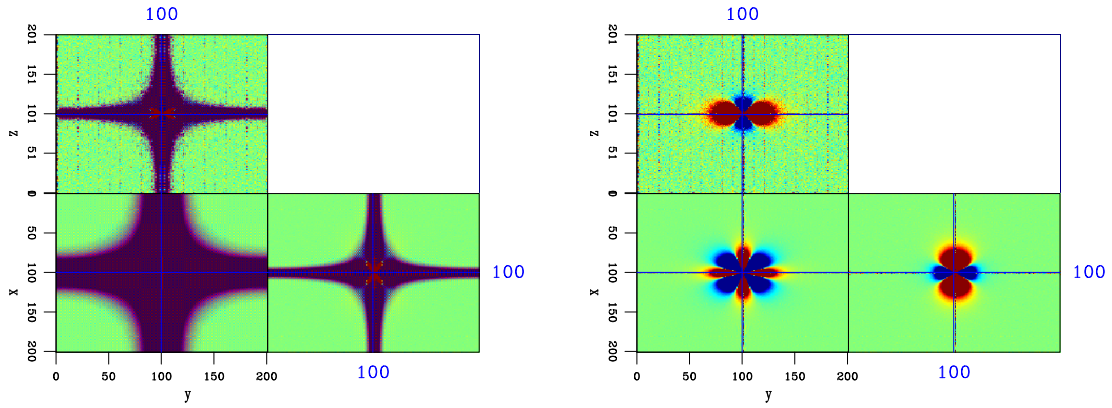

(a) (b)

Figure 4: Spatial operator that propagates just the P-wavefield: (a) with exact derivatives (equation 5) and (b) with FD approximations (equation 9). [**ER**]

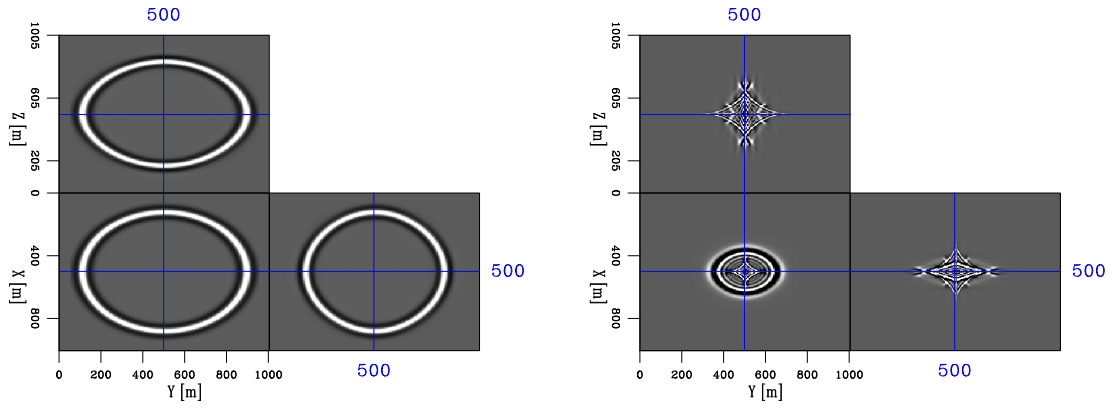

(a) (b)

Figure 5: Separated wavefields: (a) P-wavefield and (b) shear artifact modeled by spatial domain propagation (equations 8). [**CR**]

ACCURACY OF CUBE STENCILS

The operator in equation 8 can be considered as a cube stencil which is applied in the spatial domain. In order to analyze its accuracy, we compare with the conventional star stencil. More specifically, we compare the differences between a seismic trace generated by time-space domain finite differences (FD) and one generated by a time-wavenumber domain method, using the same temporal differencing (second order) and discretization steps. Figure 6(a) shows these differences for conventional star stencils of different sizes in a homogeneous isotropic medium. Figures 6(b), 7(a), and 7(b) show respectively these differences for cube stencils in VTI, weak, and strong orthorhombic media. As expected, as the size of the operator increases, the seismic traces generated by time-space domain finite differences become more accurate, i.e. approach the one generated by a time-wavenumber method. Also observed from these figures, as the degree of anisotropy reduces, a shorter operator can be used while maintaining an acceptable level of accuracy, i.e. equivalent to high-order conventional FD. In particular, 21 is a usable size for VTI media (Figure 6(b)) and 15 is usable for weak anisotropic media (Figure 7(a)), whereas strong orthorombic media might require an operator of size up to 35 (Figure 7(b)).

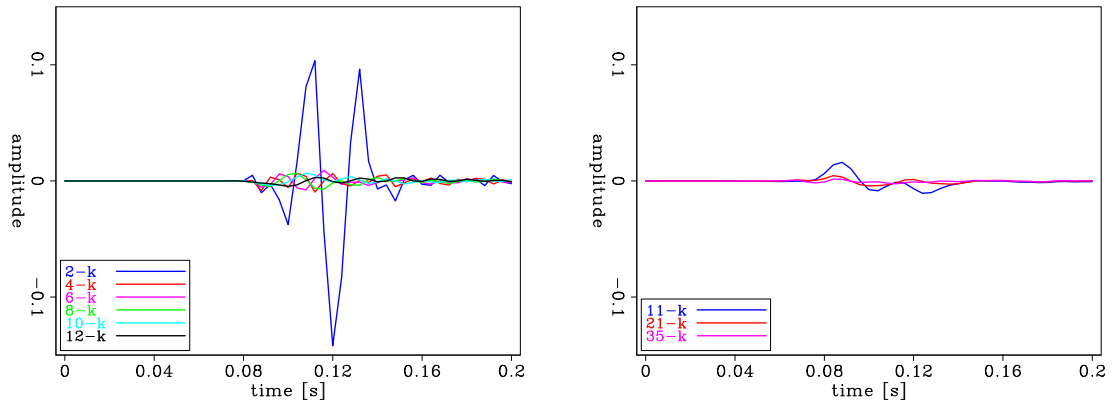

(a) (b)

Figure 6: Accuracy of different stencils : (a) Isotropic medium, conventional star stencil and (b) VTI medium, cube stencil. Legend notation $N-k$ means the difference between a seismic trace generated by a N^{th}-order FD and one generated by a time-wavenumber (k) marching scheme. [**CR**]

EXAMPLES IN A HETEROGENEOUS MEDIUM

We apply our method to an inhomogeneous medium. The model we use is 3D orthorhombic with a gradient background embedded with a wedge of higher velocity. The source is located at $x = y = 500$ m and $z = 400$ m. Heterogeneous models require an operator (equation 8) that varies spatially. This non-stationary operator is pre-computed for every model parameters to form a look-up table used during propagation. Figure 8(a) shows a slice through the velocity model and Figure 8(b) shows

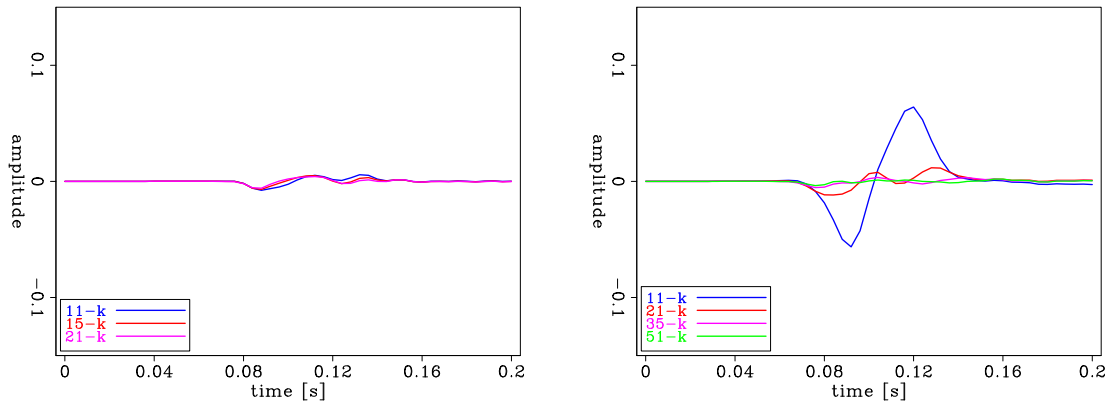

Figure 7: Accuracy of different cube stencils : (a) Weak orthorhombic medium (ϵ and δ less than 0.1) and (b) strong orthorhombic medium (ϵ and δ greater than 0.2). [**CR**]

a snapshot of the modeled wavefield. These figures show that our proposed method generates stable and artifact-free P-wavefield in heterogeneous anisotropic media.

With the operator computed for every present model parameter, application of our method in a larger and more complex case could be infeasibly expensive since it would require a huge look-up table. Our solution is to compute the operator for a number of reference models. We employ the modified Lloyd algorithm developed in Clapp (2006) for selecting model references. Figures 9(a) and 10(a) show the velocity models generated by the Lloyd algorithm with 29 and 51 references respectively. Observed in these models, the Lloyd algorithm selects the correct velocity for the wedge, but a finely-layered velocity reference for the gradient background. Consequently, the wavefields modeled with these references have artifacts. Figures 9(b) and 10(b) show the differences between the wavefields generated with these reference models and the true wavefield. The finely-layered reference background velocity generates internal reflections that are much stronger than those in the true wavefield (Figure 9(b)). Increasing the number of references helps to reduce these internal reflections. However, it boosts the transmission error (Figure 10(b)). In general, these artifacts are small in amplitude (less than 0.5%), and the main P-wavefronts modeled using the Lloyd references are virtually the same as the true one.

DISCUSSION

In 3D, the computational cost of our proposed method is quite high due mainly to the application of a dense, three dimensional convolution (equations 8). As compared to the conventional star stencil however, a cube stencil better reuses local memory and has a lower cache miss rate on high-performance computer architectures such as GPU. Additionally, the use of a lower FD order, N, or a low-rank approximation can reduce

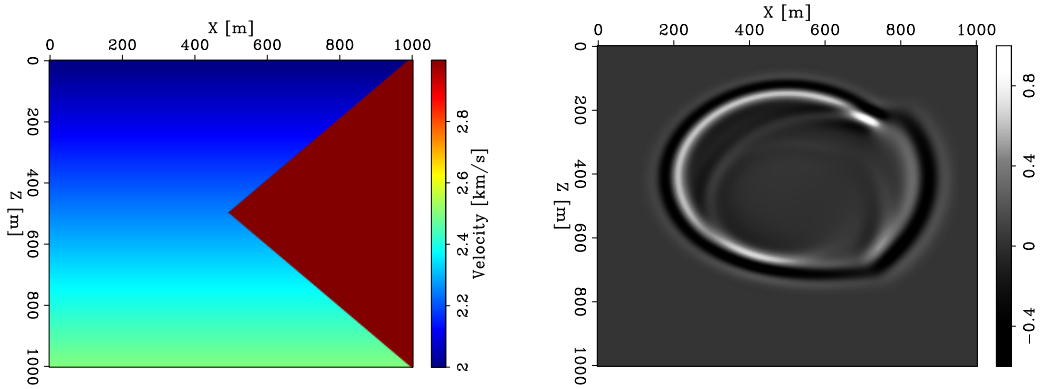

(a) (b)

Figure 8: Application of the method to an inhomogeneous medium: (a) True velocity model and (b) true wavefield snapshot. [**CR**]

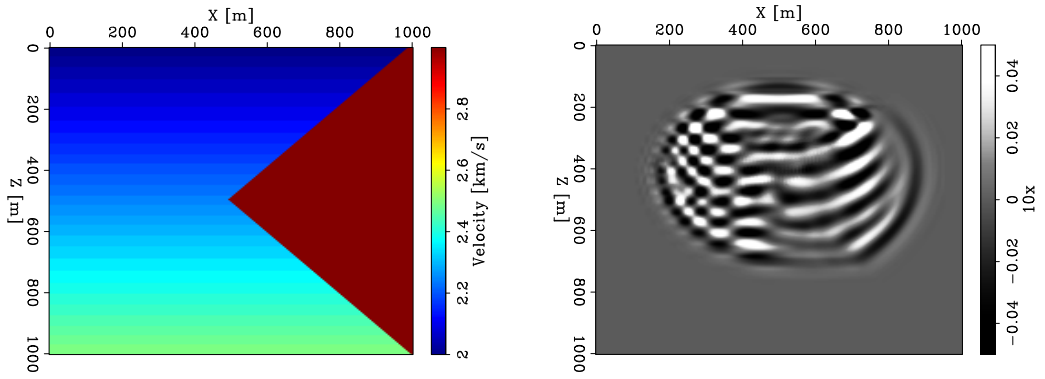

(a) (b)

Figure 9: (a) Velocity model with 29 references selected using the Lloyd algorithm and (b) difference from true wavefield (in 10x zoom). [**CR**]

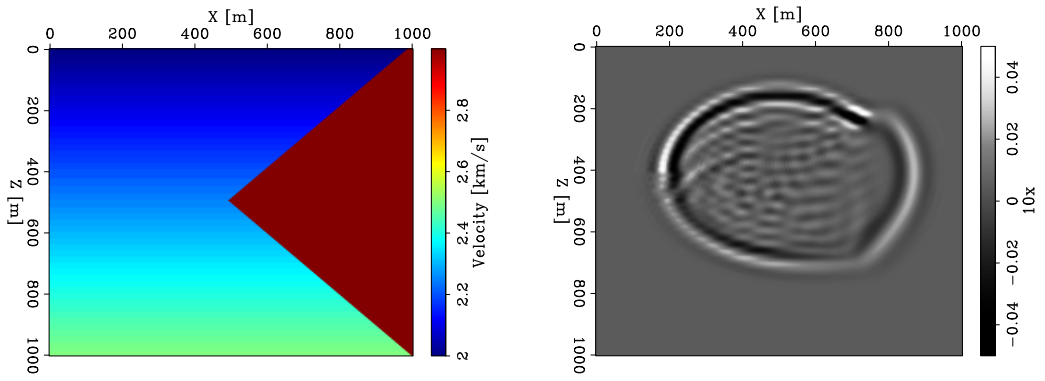

(a) (b)

Figure 10: (a) Velocity model with 51 references selected using the Lloyd algorithm and (b) difference from true wavefield (in 10x zoom). [**CR**]

the operator's size, and therefore make our method more affordable. In comparison with methods previously proposed for elastic wave-mode separation (Dellinger and Etgen (1990); Yan and Sava (2009)), our method is less expensive because it requires propagation of a single scalar field instead of a 3-component vector fields.

CONCLUSIONS

We have shown that by means of a wavenumber-domain eigenvalue decomposition of the acoustic orthorhombic wave equation's differential operator, the P-wavefield and the shear artifacts can be separated completely. The resulting eigenvalues can be used as operators to propagate the desired wavefield. These operators can be applied in wavenumber domain or inverse Fourier transformed and applied in spatial domain. Examples in homogeneous orthorhombic media validate the proposed method. We have also shown that as the degree of anisotropy reduces, a more compact, but equivalently accurate as high-order FD operator can be used. Application of our method in heterogeneous media would require interpolation or a spatially varying operator. Computing a table of operators for reference models selected by Lloyd algorithm is less expensive but produces small aftifacts. The proposed method can be also extended to elastic wave-mode separation.

ACKNOWLEDGMENTS

We would like to thank the Stanford School of Earth Sciences and the sponsors of the Stanford Exploration Project (SEP) for financially supporting this work. Thank our colleagues in SEP, especially Ohad Barak and Elita (Yunyue) Li, for many valuable discussions.

APPENDIX

In the isotropic case, $\epsilon_1 = \epsilon_2 = 0$ and $\delta_1 = \delta_2 = \delta_3 = 0$. Consequently, the density-normalized stiffness matrix, M, and the differential operator, $M\tilde{\mathbf{D}}$ respectively become:

$$M = v_{pz}^2 \begin{bmatrix} 1 & 1 & 1 \\ 1 & 1 & 1 \\ 1 & 1 & 1 \end{bmatrix}, \tag{A-1}$$

and

$$M\tilde{\mathbf{D}} = \begin{bmatrix} -k_x^2 & -k_y^2 & -k_z^2 \\ -k_x^2 & -k_y^2 & -k_z^2 \\ -k_x^2 & -k_y^2 & -k_z^2 \end{bmatrix}. \tag{A-2}$$

The differential operator, $M\tilde{\mathbf{D}}$, has three eigenvalues:

$$\begin{aligned} \tilde{\lambda}_1 &= -k_x^2 - k_y^2 - k_z^2 \\ \tilde{\lambda}_2 &= \tilde{\lambda}_3 = 0. \end{aligned} \tag{A-3}$$

The eigenvalue that is associated with P-wave is $\tilde{\lambda}_1$, which is expectedly the Fourier-domain Laplacian operator. One choice for the corresponding eigenvector is $\left[\begin{array}{ccc} 1 & 1 & 1 \end{array}\right]^T$.

The eigenvalue that corresponds to the shear artifacts is zero and has multiplicity of two. As a result, any pair of linearly independent vectors in the two dimensional subspace associated with this eigenvalue can be choosen as eigenvectors. One particular choice of those leads to:

$$\mathbf{Q} = \left[\begin{array}{ccc} 1 & k_z^2 & 0 \\ 1 & 0 & k_z^2 \\ 1 & -k_x^2 & -k_y^2 \end{array}\right], \tag{A-4}$$

and

$$\mathbf{Q}^{-1} = \frac{1}{k_x^2+k_y^2+k_z^2}\left[\begin{array}{ccc} k_x^2 & k_y^2 & k_z^2 \\ k_y^2+k_z^2 & -k_y^2 & -k_z^2 \\ -k_x^2 & k_x^2+k_z^2 & -k_z^2 \end{array}\right], \tag{A-5}$$

In the isotropic case, all three normal stresses are equal to each other and to the pressure, $\boldsymbol{\sigma} = \left[\begin{array}{ccc} p & p & p \end{array}\right]^T$, with p denoting pressure. Consequently, in the basis of row vectors of $\mathbf{Q}^{-1}$, $\tilde{\boldsymbol{\sigma}}^P = \mathbf{Q}^{-1}\tilde{\boldsymbol{\sigma}} = \left[\begin{array}{ccc} \tilde{p} & 0 & 0 \end{array}\right]^T$.

REFERENCES

Alkhalifah, T., 2003, An acoustic wave equation for orthorhombic anisotropy: Geophysics, **68**, 1169–1172.

Clapp, R. G., 2006, A modified lloyd algorithm for characterizing vector fields: SEP-Report, **124**, 249–256.

Dellinger, J. and J. Etgen, 1990, Wave-field separation in two-dimensional anisotropic media: Geophysics, **55**, 914–919.

Fletcher, R. P., X. Du, and P. J. Fowler, 2009, Reverse time migration in tilted transversely isotropic (TTI) media: Geophysics, **74**, no. 6, WCA174–WCA187.

Fowler, P. J. and R. King, 2011, Reverse-time migration in vertical and tilted orthorhombic media: 81st Annual International Meeting, SEG, Expanded Abstracts, 190–195.

Grechka, V., L. Zhang, and J. W. Rector III, 2004, Shear waves in acoustic anisotropic media: Geophysics, **69**, 576–582.

Liu, F., S. A. Morton, S. Jiang, L. Ni, and J. P. Leveille, 2009, Decoupled wave equations for P and SV waves in an acoustic VTI media: 79th Annual International Meeting, SEG, Expanded Abstracts, 2844–2848.

Tsvankin, I., 2012, Seismic signatures and analysis of reflection data in anisotropic media: Society of Exploration Geophysicists.

Yan, J. and P. Sava, 2009, Elastic wave-mode separation for VTI media: Geophysics, **74**, no. 5, WB19–WB32.

Zhang, H. J., G. Zhang, and Y. Zhang, 2009, Removing S-wave noise in TTI reverse time migration: 79th Annual International Meeting, SEG, Expanded Abstracts, 2849–2853.

Zhang, H. J. and Y. Zhang, 2011, Reverse-time migration in vertical and tilted orthorhombic media: 81st Annual International Meeting, SEG, Expanded Abstracts, 185–189.

Zhou, H., G. Zhang, and R. Bloor, 2006, Reverse-time migration in vertical and tilted orthorhombic media: 76th Annual International Meeting, SEG, Expanded Abstracts, 194–198.